Gapped metals as thermoelectric materials revealed by high-throughput screening.

Francesco Ricci[1], Alexander Dunn[2,3], Anubhav Jain[2], Gian-Marco Rignanese[1], and Geoffroy Hautier[1]

[1]Institute of Condensed Matter and Nanosciences (IMCN), Université Catholique de Louvain, Chemin des Étoiles 8, B-1348 Louvain-la-Neuve, Belgium

[2]Lawrence Berkeley National Laboratory, Energy Technologies Area, CA 94720, USA

[3]Department of Materials Science and Engineering, UC Berkeley, CA 94720, USA

July 20, 2020

Abstract

The typical strategy to design high performance thermoelectric materials is to dope a semiconducting material until optimal properties are obtained. However, some known thermoelectric materials such as La_3Te_4, Mo_3Sb_7, $Yb_{14}MnSb_{11}$, and NbCoSb are actually gapped metals, *i.e.*, their band structure displays a gap slightly above or below the band crossed by the Fermi level. This key feature makes these metals comparable to degenerate semiconductors and thus suitable for thermoelectric applications. In this work, we perform a computational high-throughput search for such gapped metals exhibiting attractive thermoelectric properties. Several thousands of metals are found to present this key feature, and about one thousand of them show decent thermoelectric properties as evaluated by a computed zT. We present the different chemistry of gapped metals we discovered such as clathrates, Chevrel phases, or transition metal dichalcogenides and discuss their previous studies as thermoelectric and their potential as new thermoelectric materials.

1 Introduction

Thermoelectric (TE) materials, which convert heat into electricity via the Seebeck effect, have attracted considerable interest as power generation devices. In addition to being scalable and reliable, TE generators are silent and require no moving parts. Sufficiently cheap and efficient TE devices therefore have massive potential to recover waste heat from a variety of industrial and consumer processes, such as automotive exhaust, home heating, and large-scale commercial processes [1–3]. However, when compared with competing technologies, industrial TE devices are both expensive and inefficient. Thus, they have been relegated to relatively niche use cases despite their potential impact.

TE efficiency is measured by the figure of merit, zT:

$$zT = \frac{S^2 \sigma T}{\kappa_{\text{lat}} + \kappa_{\text{el}}}$$

where the numerator, known as the power factor (PF), is proportional to the square of the Seebeck coefficient S, the electrical conductivity σ, and the temperature T. κ_{lat} and κ_{el} are the lattice and electronic contributions to the thermal conductivity, respectively. The sum of these two contributions is the total thermal conductivity, κ_{tot}. Optimizing zT is nontrivial, as conflicting trends in σ, S, and κ_{el} often cause one property to increase at the cost of another. Further, achieving low lattice conductivity by adjusting carrier scattering characteristics and crystal structure is highly complex. Despite these difficulties, recent investigations have developed materials with $zT \sim 2$ [4–6] by tuning at least one property among the band structure, carrier scattering, and lattice thermal conductivity [1, 6–14].

The majority of TE research is focused heavily on semiconductors. Typically, intrinsic semiconductors have a high Seebeck coefficient but low electrical conductivity. While doping can be used to increase the carrier concentration and hence σ, this consequently decreases S. Therefore, in order to approach the maximum PF, a compromise must be found between S and σ.

In contrast, despite their high electrical conductivity, metals are often disregarded as potential TE materials due to their low Seebeck coefficient. Interestingly, there are some exceptions: a few metals have a sufficiently high S to achieve high PF and zT. The most well-known are La_3Te_4 [15], Mo_3Sb_7 [16], $Yb_{14}MSb_{11}$ (M=Mn|Mg|Zn) [17–21], and NbCoSb [22, 23]. Experimental measurements show that these materials have both a low resistivity (linearly increasing with temperature) and a high Seebeck coefficient (also increasing with temperature). Such behavior is typical of degenerate (highly-doped) semiconductors. *Ab initio* band structure calculations show that, while these materials are indeed metals with some bands crossed by the Fermi level, there is an energy band gap below or above the latter. Adopting the nomenclature of Malyi et al. [24], we refer to a gap below (resp. above) the Fermi level as an internal (resp. external) gap and to these special metals as gapped metals. Their band structures, schematically illustrated in Fig. 1 for both internal and external band gap, are very similar to those of degenerate semiconductors. This similarity also holds for the transport properties (also sketched in Fig. 1). According to Mott's formula [25], a rapid variation of the Density of States (DOS) produces an increase of the Seebeck coefficient; since the presence of a band gap (in gray in the figure) makes the DOS sharply decrease, the Seebeck coefficient increases significantly and the PF presents a distinct peak. If the Fermi level is shifted (e.g., by doping) towards the band gap, the TE performances of these gapped metals can be enhanced as in degenerate semiconductors. This is in clear contrast with what happens in "regular" metals, which have a Fermi level located in an energy region where the DOS is rather constant over a wide range of energy. Thus, the presence of a gap near the Fermi level is the key feature of these special metals.

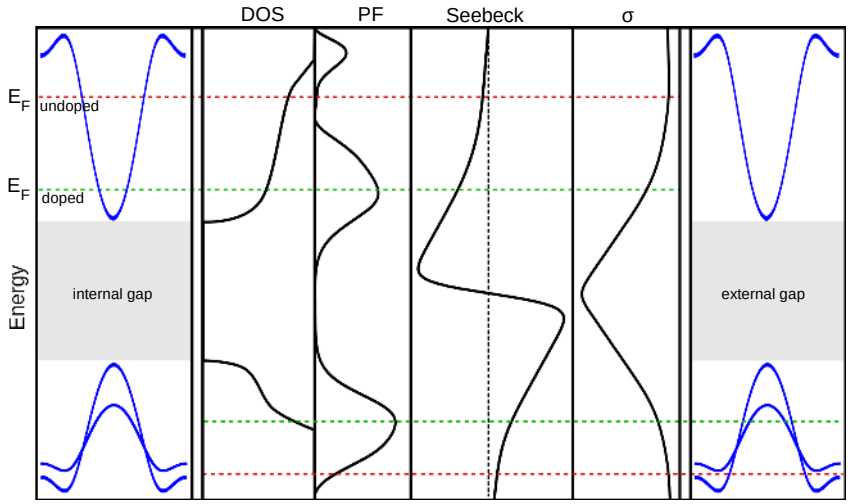

Figure 1: Sketch of the band structures of a gapped metal with internal (leftmost) and external (rightmost) band gap and of the corresponding transport properties: Power Factor (PF), Seebeck coefficient, electrical conductivity (σ). The position of the Fermi level E_{F} in the undoped (doped) case is shown with a red (green) line. In the case of an internal (resp. external) gap, the material is considered as n-type (resp. p-type).

This feature of gapped metals never been searched for explicitly in the context of TE applications. However, exceptional gapped metals have been discovered while studying chemically similar semiconductor phases; we enumerate some of these metals below. La_3Te_4 was found by investigating the metal-insulator transition from $La_{3-x}Te_4$ ($0 < x < 1$) to La_2Te_3 with La vacancies [15, 26]. The carrier concentration and hence the PF could be tuned by varying the amount of La vacancies. Metallic Mo_3Sb_7 and semiconducting $Mb_3Sb_5Te_2$ are two of the 25 compounds that crystallize in the Ir_3Ge_7 structure-type. In their solid solution $Mo_3Sb_{7-x}Te_x$, the Te concentration allows the tuning of the Fermi level towards a high ZT [16]. All the $Yb_{14}MSb_{11}$ (M=Al|Mn|Mg|Zn) compounds, which belong to the 14-1-11 Zintl family [27], present a stable phase with comparable band structures. However, while the Al-based compound is a semiconductor, the other three are metals [18, 20, 28]. The notable difference in the band structure of the latter compounds is that the Fermi level is inside the valence bands, but an external band gap (corresponding to the one of the Al-based compound) is present. Experiments showed that a metal-insulator transition takes place when replacing Al with Mn. This can be exploited to tune the PF by moving the Fermi level while the bands remain essentially unchanged [19]. The half-Heusler NbCoSb has been recently discussed in terms of odd valence electron count [23]. While many half-Heusler compounds have 18 valence electrons which fill the bands [29] and hence induce semiconducting behavior, NbCoSb has 19 valence electrons. The 19th electron starts filling the conduction band and leads to a metallic character. Experimentally, this compound is stabilized by Nb vacancies and approaches the 18-electron configuration. In the same family, VCoSb was also proposed, and experimental measurements confirm a high PF value [30]. In these cases, both the vacancies (as in La_3Te_4 and NbCoSb) or the complex crystal structure (as in Mo_3Sb_7 and $Yb_{14}MSb_{11}$) turn to have also the beneficial effect of reducing the lattice thermal conductivity and improved zT.

Not only has the presence of an internal or external gap in metallic system never been searched explicitly, it has also been often overlooked. For example, Parker et al. [31] considered NiSbS not worthy of further investigation because it was predicted to be metallic, yet they did not realize that the presence of an internal band gap could have an impact on the transport properties. Four years later, the same material NiSbS was studied by Miyata et al. [32], and a high PF was measured.

In order to adopt a more systematic approach for finding gapped metals, modern high-throughput (HT) density functional theory (DFT) is of particular interest. HT-DFT gives access to a large quantity of computed properties for thousands of materials [33–35] and enables the search for specific features. This approach is effective in performing large scale investigations, discovering new materials, and enabling the use of machine learning techniques in various sub-disciplines of material science [36–38]. In the search for new TE materials, recent HT investigations have, however, focused on semiconductors, imposing a threshold on the band gap value [39–42, 42, 43], and therefore disregarding metallic compounds.

In this work, we use a database of band structures built by HT computing to detect these exceptional metallic compounds presenting a band gap close to their Fermi level. We show that these gapped metals are common and can be found in a large variety of chemical systems, compositions, and space groups. By looking at their transport properties, computed with a constant relaxation time, we show that about one thousand materials can reach moderate theoretical zT values when the chemical potential is shifted towards the energy gap, e.g. by doping. We discuss the candidates previously studied in the literature and propose some new potential TE materials for further investigation.

We note that there is precedent for probing these gapped metals for functional applications other than thermoelectrics. The presence of a gap close to the Fermi level in metallic systems and its influence on the electronic and optical properties has been already discussed mainly in the field of transparent conductive oxides [24, 44–47] and recently for applications in low-loss plasmonics [48]. Therefore, given that this key feature of the band structure can potentially be exploited for other applications, we report all the gapped metals found by this screening along with their calculated properties (in SI).

2 Screening method

In order to identify metallic compounds with transport properties of interest, we screen the Materials Project (MP) database [33] for metallic compounds whose band structures are present in the dataset of Ref. [49] (∼15,000 materials, while there are ∼20,000 in the complete MP dataset as of today). Extensive details on the band structure calculations are available in their original publications [49, 50]. Most band structures considered here were computed using the generalized gradient approximation (GGA), while only a few compounds (e.g., metallic transition metal oxides) used the $+U$ correction (GGA+U). Candidate materials are identified by searching for band gaps in a range of 4 eV centered on the Fermi level and retaining only the closest one. In the case of an internal (resp. external) gap, the material is considered as n-type (resp. p-type).

Furthermore, a constraint is imposed in terms of stability by retaining only the phases with an energy above the convex hull lower than 0.05 eV/atom. This value accounts for the inherent error

of DFT in evaluating the stability of compounds [51]. We note that thermodynamic instability at the theoretical composition has often been observed experimentally in the class of materials we are discussing. For example, NbCoSb is likely unstable due to a reported energy above Hull of about 0.02 eV/atom in MP. Experimentally, Nb vacancies are found to stabilize the compound and also increase the PF. Other examples include Chevrel phases and clathrates which possess an energy above hull higher than 0.05 eV/atom yet are experimentally accessible.

The transport properties reported in Ref. [49] were calculated relying on the constant relaxation time approximation (CRTA) using the BoltzTraP code [52]. While in that dataset the properties were reported divided by the value of the relaxation time, here we set its value to $\tau = 10^{-14}$ s, as commonly used. We focus on the averages of the eigenvalues of the PF, the Seebeck coefficient, the conductivity, the electronic contribution to the thermal conductivity, and the carrier concentration at 4 temperatures (300, 600, 900, and 1200 K). The ranking of the different materials is based on the optimal value of the PF. The optimal PF is determined as its maximum value in the energy range between the Fermi level and the band edge (the conduction or valence band maximum, VBM and CBM, respectively) if the corresponding carrier concentration is lower than 10^{22} cm^{-3}. Otherwise, the PF value at a concentration of 10^{22} cm^{-3} was taken. For the other transport properties, we retain the values at the chemical potential corresponding to the optimal PF. This constraint on the carrier concentration allows us to consider a PF which is more likely to be reachable via doping without destabilizing the host.

It is worth noting that the transport properties of NbCoSb are not in the dataset of Ref. [49] and that the band structure of $Yb_{14}MnSb_{11}$ is not currently available in the MP database. Given the importance of these two materials as benchmark for our screening, we added them separately by calculating the band structure and the corresponding transport properties with the same methodology used for the other materials.

In order to assess an approximate zT, a minimum limit for the lattice thermal conductivity is derived from the calculated elastic constants reported in the MP database. Details regarding the elastic constant DFT calculations are available in Ref. [53]. Since the calculated elastic constants are not available for all the compounds in the MP, a machine learning (ML) model is used to predict the missing values. A general-purpose materials data mining package (Matminer [54]) and its AutoML extension (Automatminer [55,56]) are used to train, validate, and deploy the model. Automatminer automatically searches multiple machine learning models (including hyperparameters) and descriptor-generation (featurization) techniques to optimize end-to-end data pipelines for predicting materials properties directly from crystal structures. Separate AutoML pipelines are developed to predict shear and bulk moduli independently, and both pipelines are trained on DFT-computed elastic constants from the MP. The best pipelines found by the AutoML algorithm use subsets of compositional and structural descriptors such as MagPie [57,58] elemental statistics, Sine Coulomb Matrix [59] eigenvalues, and elementary symmetry and density descriptors. These descriptors are used as input to the optimized models found by AutoML: Extra Trees and Gradient-boosting trees models for predicting shear and bulk moduli, respectively. Exact sets of descriptors and final pipeline hyperparameters are available in the supporting information (SI Section 2 an relative Tables). Using the elastic constants calculated by DFT and ML, the Cahill-Pohl [60,61]

lower bound on lattice thermal conductivity in the high temperature (glassy) limit is calculated using the approach of Ref. [40]. The ML model produces elastic constants resulting in a minimum lattice thermal conductivity mean absolute error of $0.061 \mathrm{W/m \cdot K}$ (test set mean average deviation of $0.370 \mathrm{W/m \cdot K}$); this error was computed using 20% test sets of DFT-computed elastic moduli as ground truth. Further details on this method are provided in Sec. 2 of SI.

Combining together these computed quantities, an approximated optimal zT is calculated and used for the final ranking of the compounds. A zT=0.2 threshold at 600 K has been set to separate the interesting candidates from the rest, as discussed in the next section.

Before discussing the results of the screening, we would like to emphasize the main limitations of our approach. The major approximation is the use of the CRTA, an approach which neglects the formal dependence of the relaxation time on the energy and the wavevector. This is a necessary choice for calculating transport properties on a large scale, as any other scattering model either requires a large computational time or is material-dependent. Though CRTA yields transport properties that do not always match the experimental values, it remains a valuable method, especially for ranking materials [40, 49]. The other limitations are related to the accuracy of the band structures, in particular the use of the GGA functional and of pseudopotentials for Rare-Earth (RE) elements. The GGA functional is known to underestimate the band gap [62]. Though this is not an issue for the assessment of zT given that a larger gap is generally beneficial for the Seebeck coefficient, it can still lead to some false positives in our screening process. Indeed, when d-orbitals are involved, GGA may predict a material to be metallic, while more advanced functionals would show that it is actually semiconducting (with a non-zero gap). This problem will be discussed further in the following sections.

Similarly, the use of a single pseudopotential for each element (necessary for the HT approach) can also lead to false positives when RE elements are present. Indeed, the latter often have multiple oxidation states which may not be well represented by a single pseudopotential (in particular, for oxidation states that make one of the frozen electron participate in bonding). These types of false positives were also found during the screening process and will be discussed in the following sections.

Finally, another possible issue with compounds containing RE elements relates to the positions of f-electrons which are often not well described within standard GGA. It is therefore reasonable to expect a few discrepancies with respect to experiments. In some cases, both more accurate functionals, e.g La_3Te_4 [63], and experimental measurements, e.g. $Yb_{14}MnSb_{11}$ [64], show that f-electrons are far from the Fermi level and do not contribute significantly to transport properties. In other cases (e.g. Pr_3Te_4 [63]), the f-electrons can be close to the Fermi level (and hence to the band gap) enhancing the variation of the DOS and the Seebeck. We chose to retain the RE-containing materials with the caveat that more accurate calculations might be needed for those cases in order accurately locate the f-electrons and assess their impact on transport properties.

3 Results and discussion

Our band structure screening reveals that, among the ∼15,000 metallic compounds considered in this screening, about 30% present at least one band gap within 2 eV of the Fermi level. As a first result, it is notable that this key feature is surprisingly common in metals. In Fig. 2, we report the calculated PF, the total thermal conductivity, and the estimated zT at 600 K for the materials remaining after the screening based on stability. We also plot these properties (computed in the same way) for the most well-known TE materials, both metals and semiconductors. The use of a single temperature eases the comparison between many compounds. The temperature of 600 K is a good compromise to find a moderate zT for compounds that have typically the best zT at very different temperatures (i.e. Bi_2Te_3 and $Yb_{14}MnSb_{11}$ at 300 K and 1000 K, respectively). This comparison is used to validate our approach representing a benchmark for assessing the quality of the ranking obtained by the screening method. As shown in the plot, the most well-known TE materials all have high values of calculated zT. Therefore, it may be assumed that this screening provides an approximately correct ranking of TEs, despite the strong approximations involved. It is reasonable to expect that the best gapped metal TEs will reside in the same zone of the plot as the most well-known TEs. By also considering the uncertainty in the computed zT, a value of 0.2 at 600 K for the calculated zT can be chosen as a threshold to separate those compounds that are likely to be more promising from the rest. We would like to stress again that this computed zT is used as a descriptor to rank materials and detect promising compounds. Therefore, it is not necessarily expected to agree with the measured zT value, as it will be shown later. After setting this threshold of the zT, 1156 gapped metals remained. In Table 1, they are reported according to the number of elements in the chemical system.

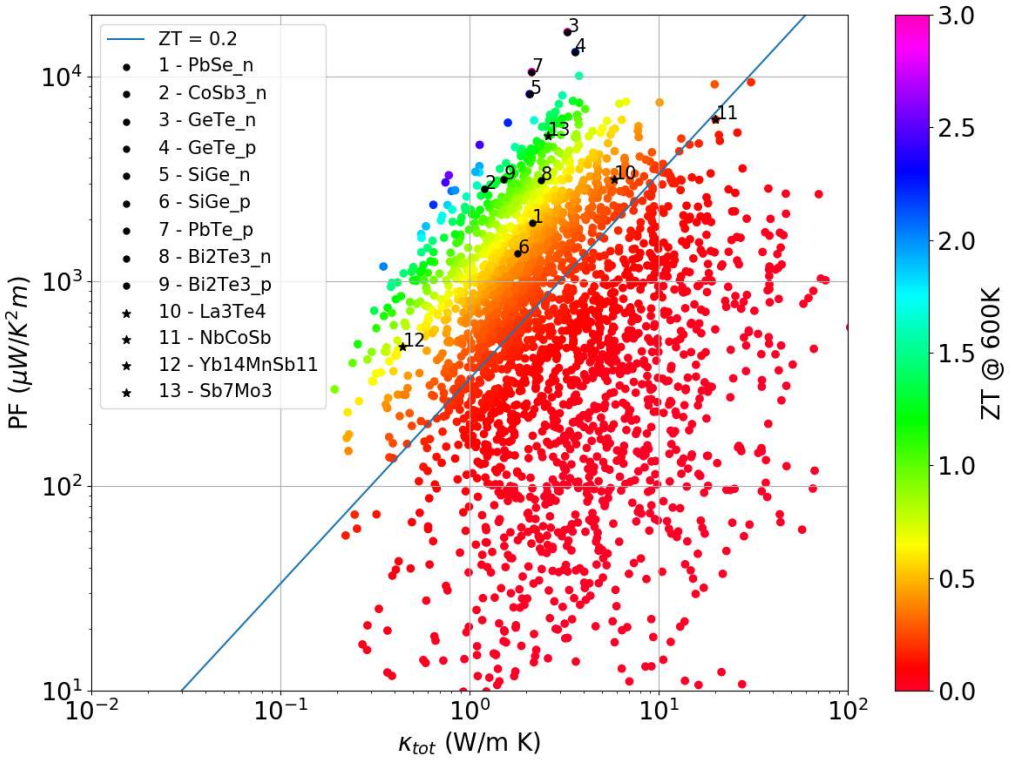

Figure 2: Values at 600 K of calculated total thermal conductivity κ_{tot}, computed optimal PF and zT for all the gapped metals and energy above Hull lower than 0.05 eV/atom. Star markers represent the TE materials considered here as reference, dot markers represents other known TE materials. The blue solid line represents the chosen threshold of zT=0.2.

	$zT > 0.2$
binaries	141
ternaries	624
quaternaries	314
quinaries	77
total	1156

Table 1: Number of compounds with computed optimal $zT > 0.2$ at 600 K.

In order to get a sense of the discrepancies between the calculated values of the transport properties and the experimental measurements, we consider four of the most well-studied gapped metal TEs: La_3Te_4, Mo_3Sb_7, $Yb_{14}MnSb_{11}$, and NbCoSb. According to the transport properties at 600 K reported in Table 2, the predicted optimal zT of La_3Te_4 is in agreement with the experimental value, even if by serendipity. For Mo_3Sb_7, the calculated optimal zT overestimates the experimental value by nearly 600%, mainly because the theoretical optimal carrier concentration is higher than the experimental one, leading to a higher expected Seebeck coefficient. In the case of NbCoSb, the calculated transport properties disagree with experiment via a mismatch in the carrier concentration; the calculated optimal zT

is nearer to the experimental value (within 50%) only by chance. For $Yb_{14}MnSb_{11}$, a good agreement is found for all the transport properties, but the optimal carrier concentration is quite different. This comparison shows that the match between calculated and experimental transport properties is not perfect. The use of experimental carrier concentration to compute the transport properties does not always improve the accuracy. This is certainly related to the approximations used in the calculations, but also to the fundamental difference between theoretical crystalline compounds and experimental samples that makes the comparison even more difficult. Therefore, we emphasize that the computed values of zT reported here are not intended to predict the real ones, but rather to rank materials, suggest potential candidates, and understand general trends [40].

Compound		n	S	σ	κ_{lat}	κ_{el}	κ_{tot}	zT
La_3Te_4	th.@opt.	2.2	86	4.0	0.4	5.4	5.8	0.3
	th.@exp.	0.2	133	0.8	0.4	1.18	1.58	0.6
	exp. [26]	0.2	215	0.1	—	—	0.6	0.4
Mo_3Sb_7	th.@opt.	0.9	162	2.0	0.7	1.9	2.6	1.2
	th.@exp.	4.0	60	6.8	0.7	7.0	7.7	0.2
	exp. [16]	4.0	100	0.9	1.7	1.5	3.2	0.2
NbCoSb	th.@opt.	8.6	64	15.0	0.9	19.0	19.9	0.2
	th.@exp.	5.5	85	10.0	0.9	13.0	13.9	0.3
	exp. [22]	5.5	140	0.7	2.7	—	3.9	0.3
$Yb_{14}MnSb_{11}$	th.@opt.	0.1	194	0.1	0.4	0.1	0.5	0.6
	th.@exp.	0.5	40	0.5	0.4	0.3	0.7	0.1
	exp. [19]	0.5	146	0.2	—	—	0.7	0.4

Table 2: Comparison between theoretical (th.) and experimental (exp.) transport properties (Seebeck coefficient S in μV/K, electrical conductivity σ in 10^5 S/m, and thermal conductivity κ in W/(K m)) at 600 K for four known gapped metallic TE materials. The theoretical transport properties are reported for both the optimal (@opt.) and experimental (@exp.) carrier concentrations (n in 10^{21} cm^{-3}) are reported. For the thermal conductivity, κ_{lat} is the lattice contribution (either the experimental value or the theoretical minimum limit in the Cahill model) and κ_{el} is the calculated electrical contribution.

With our approach, it is still possible to observe the importance of the presence of a band gap close to the Fermi level. As shown in Fig. 3 (and extensively in SI Figs. 3,4,5,6), in all these phases, the calculated optimal PF increases with temperature as expected from the presence of the band gap. This is mainly due to the increase of the Seebeck coefficient with temperature which drives the increasing of the PF. The presence of a nearby band gap is a fundamental reason why the known gapped metals have high experimental zT ($\sim$1) at high temperature ($\sim$800-1200 K). This behavior can be extended to nearly all the gapped metals found by this screening. Indeed, as shown in SI Table 6, 99% of the materials with $zT > 0.2$ reach their maximum optimal zT at temperature higher than 300 K.

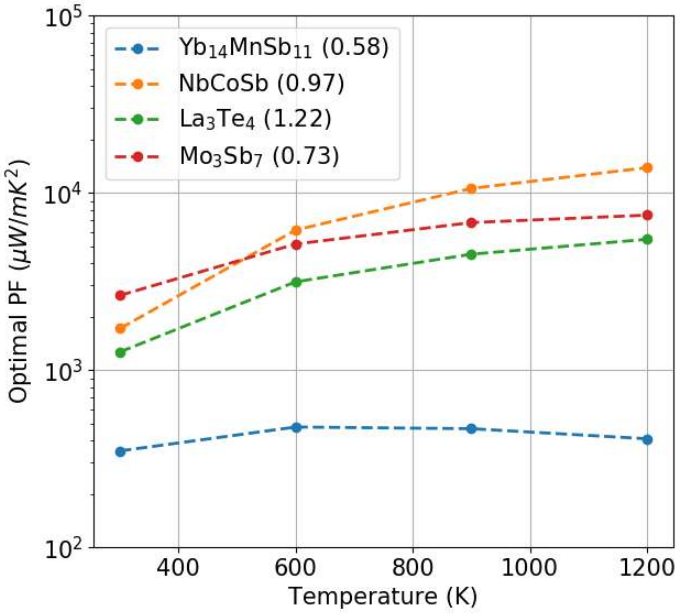

Figure 3: Calculated optimal PF w.r.t. to the temperature of the four known gapped metallic TEs . In the legend, the band gap is reported in eV.

Doping is the other way to move the Fermi level towards the band gap while increasing the PF. A general trend for ternaries is shown in Fig. 4 using histograms of the position of the Fermi levels in the undoped and optimized (i.e., in the sense of optimal PF used in this screening) compounds. In SI Figs. 1 and 2 similar histograms are shown for all the other compounds. In Fig. 4(a), without filter on the computed zT, the undoped compounds have a flat distribution of the Fermi level positions (histogram bars in blue), while in the case of the optimized compounds the Fermi level has moved towards the VBMs or CBMs (histogram bars in orange). This effect is even more pronounced if the limit on the carrier concentration is removed (histogram bars in green), with most of the compounds having a Fermi level at a distance lower than 0.5 eV. Furthermore, in Fig. 4(b) we show this effect holds particularly for those gapped metals with an optimal computed zT higher than 0.2. The distribution for the undoped case is less spread than in the case without zT the zT filter. This means that the Fermi level is already quite close to the band gap in those gapped metals that reach a high zT with a limited carrier concentration. Looking at the PF and the band structures reported in SI for most of the materials discussed later, it can be observed in details that the PF usually peaks close to the beginning of the band gap (VBM or CBM), whereas it decreases going inside the bands.

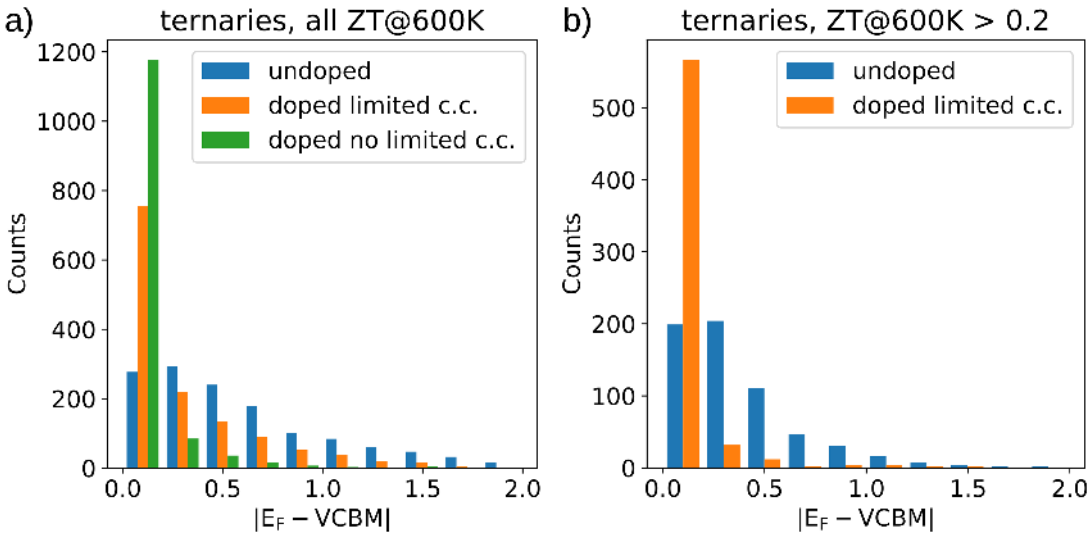

Figure 4: Distribution of the Fermi level in the gapped metals (a) with no filter on the optimal zT applied and (b) with a optimal $zT > 0.2$ at 600 K. VCBM stands for VBM (CBM) in case of an external (internal) gap. Blue bars represent the undoped state, the orange bars the optimized case with the limit of the carrier concentration at 10^{22} cm^{-3}, and green bars the optimized case without that limit.

We now discuss the other gapped metals with calculated $zT > 0.2$ at 600 K and compare them with observations from literature. A comparison with the studies presented in literature allows us to validate the present screening, highlight some limits, and suggest some overlooked metals as potential thermoelectric materials. Among all the compounds found in this screening, we will discuss here those belonging to the well-studied families of TE compounds, and we point out others that are interesting yet less studied for TE applications. Given both the breadth and raw number of compounds, we focus only on binaries and ternaries. Also, we tend to discard the compounds with a complex band structure, i.e., those which have mixed flat and dispersive bands or which have strong features giving a high calculated optimal PF far from VBM or CBM. While these could be promising compounds for TE applications, they are beyond the simple scheme of the gapped metals discussed here. Examples are Cl-, Br-, I-based compounds reported to have quite high optimal PF and very low κ_{tot} (see $RuBr_3$, mp-23294, space group *Cmcm*, shown in SI Fig. 7).

3.1 Binaries

We begin by discussing the binary compounds in the order in which they appear in Table 3.

Clathrates

The first group of compounds belongs to the clathrates family [65]. The general formula of type-I clathrates is A_8X_{46} where X is Si, Ge, or Sn and A is a guest atom, such as Na, K, Ba, or Cs. They are usually unstable metallic phases in full stoichiometry, where vacancies, group 13 elements (Al, Ga, or In), or transition metals are used to replace X site to stabilize the structure. We note that important clathrates as Ba_8X_{46} with X=Si, Ge are not found in our screening because they have a high energy above Hull

($>$ 0.05 eV/atom). The more stable phases here reported show n-type carriers, a quite small computed thermal conductivity ($\sim$1 W/(K m)), and a moderate PF ($\sim$30 μW/(K^2 cm)). As examples, the crystal structure of K_4Ge_{23} is shown in Fig. 8, its band structure and its computed transport properties are shown in Fig. 5. Clathrates have been studied for TE applications [66, 67] mostly because of their low thermal conductivities, a phenomenon often related to the phonon glass–electron crystal concept [68]. Another fundamental characteristic is the high chemical tunability that can change these phases from being metals to both n- and p-type semiconductors. This can be understood using the Zintl concept as explained in Ref. [66]. Among the most well-known is $Ba_8Ga_{16}Ge_{30}$, which reaches a $zT \sim 1.35$ at 900 K [69]. $Ba_8Ga_{16}Ge_{30}$ combines a low thermal conductivity with a high Seebeck at high temperatures - high Seebeck with increasing temperature is a sign of the presence of a band gap. The Fermi level tunability of Cs_8Sn_{46} with Sn vacancies or replacing Sn with Zn or Ga was theoretically investigated in Ref. [70]. Also, the band gap assessment of $K_8Ga_8Si_{38}$ by optical measurement was reported in Ref. [71]. Moreover, as shown in Ref. [72], the inclusion of Ni atoms in Ba_8Si_{46} moves the Fermi level towards the band gap and increases the PF and the zT. However, including Ni also completely changes the bands near the band gap edges. The tunability of the band gap with transition metals is reported in Ref. [73]. The research in clathrates is still active, indeed a new stable phase $Cs_8In_{27}Sb_{19}$ with a high Seebeck and mobility was recently reported [74].

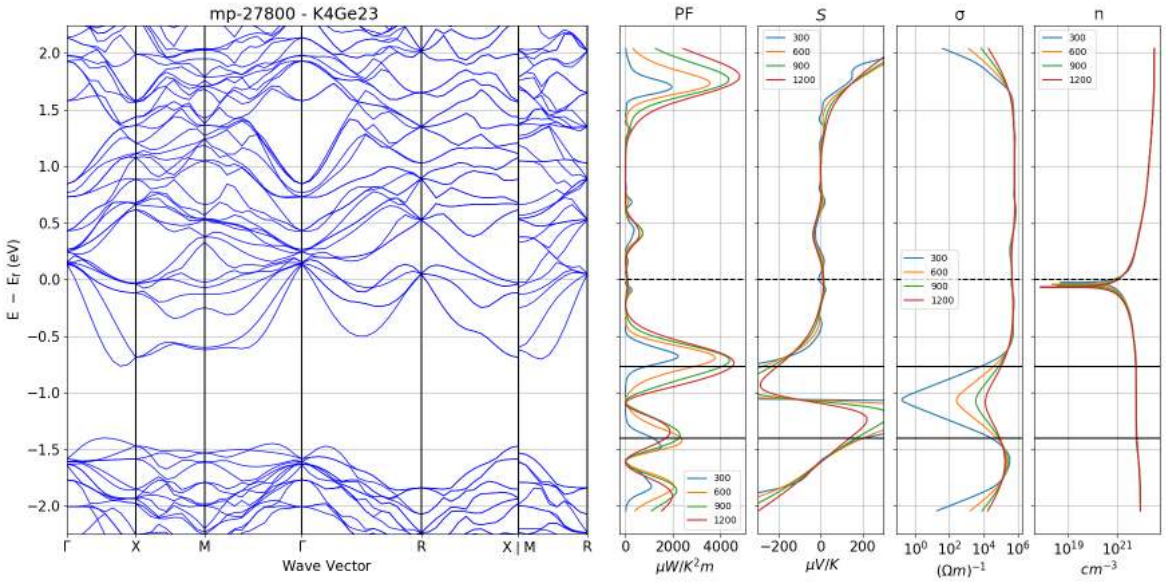

Figure 5: Band structure and calculated transport properties of the clathrate K_4Ge_{23} (mp-27800).

Transition metal dichalcogenides

The compounds with space group *P6$_3$/mmc* and composition 1-2 include NbS_2 and TaS_2, predicted here to be n-type with a high optimal zT ($\sim$0.7 and $\sim$0.3 respectively). These compounds are known transition metal dichalcogenides and are in the same family as the known semiconducting MoS_2. NbS_2, TaS_2 were reported as metals in Ref. [75]. Taking the band structure of NbS_2 in Fig. 6 (crystal structure

in Fig. 8) as representative of the two (see SI Fig. 9 for TaS_2), a band gap above and a second one below the Fermi level are found. Here we report the calculated optimal zT in the hypothesis of moving the chemical potential towards the closer band gap, the one below the Fermi level. In the case of $NbSe_2$ (SI Fig.10, the lower band gap is closed, therefore the upper band gap is taken into account by our screening and the material is considered p-type, but with a low zT (<0.1). In the literature, the existence of one or two band gaps in these materials was recently considered for optical applications in Ref. [76]. A low Seebeck coefficient was reported in Ref. [77] for NbS_2 with Li intercalation. Moreover, calculated band structure using HSE confirms the presence of the two band gaps for TaS_2 [48]. Electron-phonon scattering in TaS_2 was recently studied theoretically [76], but no Seebeck coefficient was reported. In general the effect of the doping on the Seebeck coefficient seems not to have been investigated extensively in this class of metallic compounds.

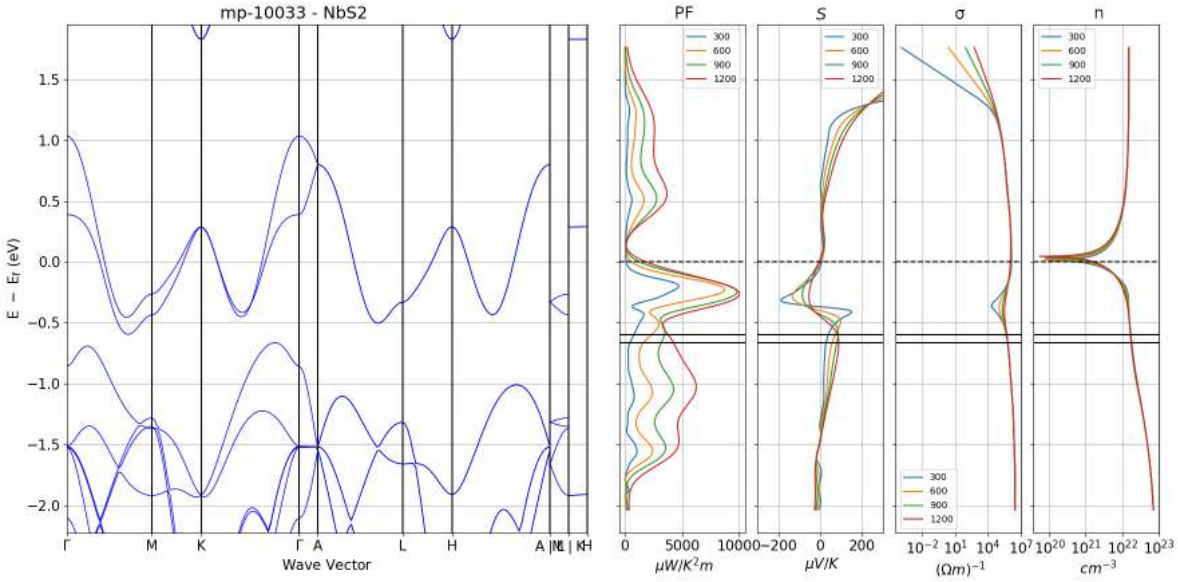

Figure 6: Band structure and calculated transport properties of the transition metal dichalcogenide NbS_2 (mp-10033).

The effect of Ta doping on the transport properties of TiS_2 (SI Fig. 11) was investigated in Ref. [78]. TiS_2 reaches a zT value close to 0.4 at 700 K, and various nanostructuring techniques are reported to decrease its thermal conductivity by exploiting its layered structure. The pristine TiS_2 compound shows an n-type behavior. Ta doping decreases the negative Seebeck coefficient and increases the conductivity with a PF found at 7 μW/(K^2 cm). This material is found by the present screening because the band structure shows a band gap near 2 eV above the Fermi level. However, the calculated optimal PF (∼50 μW/(K^2 cm), reported by this screening) is actually much closer to the Fermi level than to the gap. This is likely due to the particular shape of the bands that include a pseudo-gap around the Fermi level (see SI Fig. 11).

La_3Te_4 family

Among the binaries, we also note the large family of 28 phases with the same stochiometry and space group ($I\bar{4}3d$) of La_3Te_4. Most of these 3-4 phases have similar n-type band structure, yet 5 show a vertically mirrored band structure with the Fermi level in the valence band just below the VBM at Γ. In Fig. 7 we report the band structure and the calculated transport properties for the interesting case of Ba_4Bi_3, along with its crystal structure in Fig. 8. In Ref. [79], Ba_4Bi_3 is reported to be stable and to have good metallic conductance. Notably, in Ref. [80], Bi vacancies are reported to form spontaneously to increase the stability of the material. This is actually beneficial for the TE properties; since vacancies cause the holes in the valence band to be filled and move the Fermi level towards the band gap, Bi vacancies actually improve the PF. More recently, topological behavior was discovered in this compound due to band crossing near the Fermi level [80,81]. To our knowledge, this system has not been investigated as a thermoelectric material.

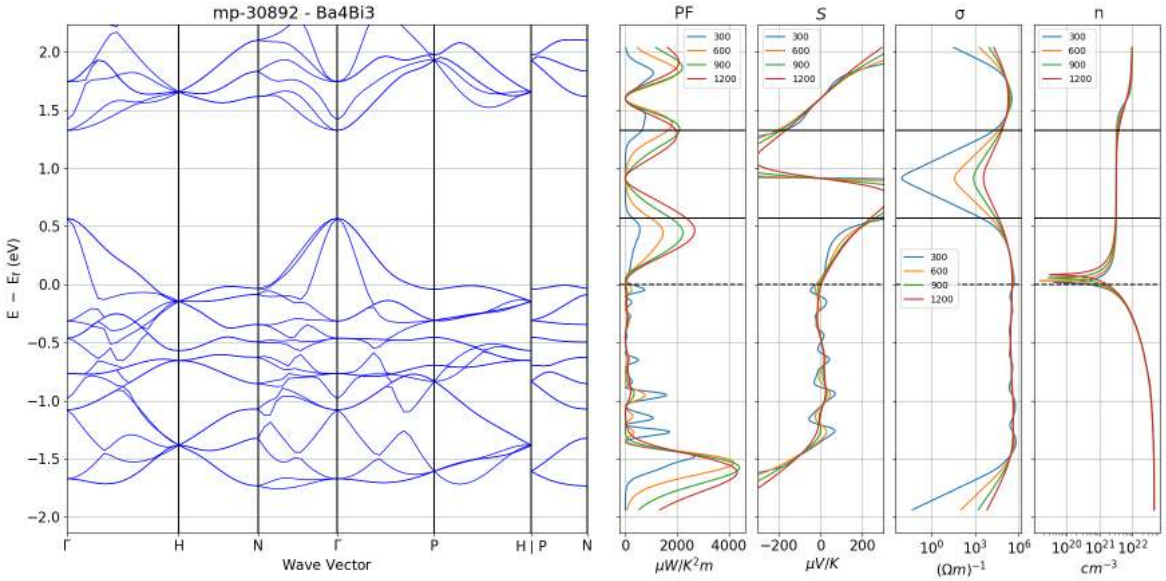

Figure 7: Band structure and calculated transport properties of Ba_4Bi_3 (mp-30892).

Others

In Ref. [82], a metal-semiconductor transition via Ru doping of In_3Ir has been reported. The chemical doping with Ru ($0 < x < 1$) shows a drastic change in the transport as expected by the presence of the band gap. The low conductivity, however, limits though the value of zT to 0.05. The presence of a flat band just above the CBM could be the origin of the low conductivity. In SI Fig. 12, the band structure and the computed transport properties are shown for In_3Ir. A similar metal-semiconductor-metal transition has been studied in $Fe_xCo_{1-x}Si$ and $Fe_xMn_{1-x}Si$ alloys [83]. The compounds at the extremities, MnSi and CoSi, are both found in our screening as gapped metals, while FeSi is a small band gap semiconductor. They have a very similar band structure, but are distinct due to position of the Fermi level: in CoSi, the Fermi level is above the band gap, while it is below the band gap in MnSi, as

shown in SI Figs. 13 and 14. The optimal computed zT is quite low for both due to their high minimal thermal conductivities and low power factors. The PF can be improved if the constraint on the carrier concentration is dropped, i.e., the Fermi level is allowed to reach the band edges. In similar cases of alloys of two gapped metals, the limit on the carrier concentration used in this screening might be dropped.

Yb_5Si_4 and Yb_5Ge_4 appear to be metallic in our screening but experimental measurements showed a typical semiconducting behavior of the resistivity [84]. In these materials, Yb has mixed valence (+2 and +3) depending on the site it occupies, which leads to a completely filled valence band. On the contrary, the band structures used for this screening were calculated with a Yb pseudopotential with only two f-electrons (simulating the +2 valence), thus the valence band is not filled and the material is a metal. On the one hand, this represents a case where our approach fails; on the other, it shows that the screening sheds light on materials that were probably overlooked as TE materials. Indeed, Yb_5Si_4 and Yb_5Ge_4 are not extensively studied: no accurate band structure has been reported and no Seebeck coefficient measured to our knowledge. As shown in SI Fig. 15, assuming this compound as semiconducting, Yb_5Si_4 shows an interesting conduction band with high computed optimal PF (~30 μW/(K^2 cm)). We note that its GGA band gap is quite small ~0.08 eV, but use of a better functional may compute a larger gap.

$Li_{15}Si_4$ is a crystalline phase that appears when increasing lithium concentration in silicon anode of lithium ion batteries [85]. To our knowledge, this system has not been investigated as a thermoelectric material. Its band structure and transport properties are shown in SI Fig. 16.

A series of interesting binaries gapped metals found in this screening but not reported in literature as TE materials are listed in the last two sections of Table 3. Their band structures and transport properties are reported from Fig. 17 of Sec. 7.1 of SI.

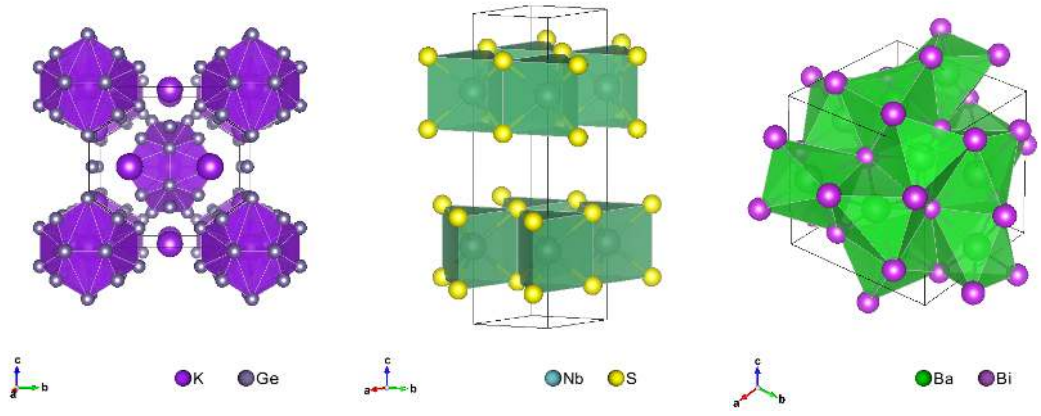

Figure 8: From left to right, the crystal structure of K_4Ge_{23}, NbS_2, and Ba_4Bi_3.

3.2 Ternaries

In the following, we continue discussing the ternary compounds in the order in which they are listed in Table 4.

Chevrels

The compounds in the second group are rhombohedral ternary chalcogenides of formula $M_xMo_6X_8$ (X = chalcogen, M = Cu, Ag, Ni, Fe, Ti, rare-earth, etc.) known as Chevrel phases [86]. The common building block Mo_6X_8 is arranged in such a way that leaves space in the structure for inserting additional metal atoms (M) of a large variety of species. The choice of filling atom is crucial in determining the structural and electronic properties of these phases. The phases reported here show p-type carriers, a very small computed thermal conductivity (< 1 W/m K), and a moderate computed PF ($\sim$30 μW/(K^2 cm)). As an example, the band structure and the computed transport properties are shown for $Ca(Mo_3S_4)_2$ in Fig. 9, while its crystal structure is in Fig. 12. These phases have been studied mostly for their remarkable superconductivity [87], but also for their good TE [88–93] and catalytic [94] properties. The most studied phases for TE applications have transition metals on the M atom. Given their small size, they can fill most of the empty sites in the structure, leading to a fine tuning of the carrier concentration. Although other species, e.g. La, Pb, can be used to tune the Fermi level, they can only fill some of the empty sites due to their bigger size, resulting in reduced tunability. This explains the existence of the Chevrel compounds $Cu_4Mo_6S_8$ with 4 Cu filling atoms, and $LaMo_6S_8$ with only one La filling atom. They show positive Seebeck coefficient, low-to-medium conductivity, and low thermal conductivity resulting in a best zT that ranges from 0.17 to 0.4 at high temperatures $\sim$1000 K. It appears that the low thermal conductivity stems from filling atoms that enhance the phonon scattering. The increasing Seebeck coefficient with the temperature is likely due to the near band gap. Disappointingly, experimental data show both Seebeck coefficient and electrical conductivity are not high enough to reach a good PF. Theoretical work suggests that the electronic performances and mobility could demand on the type of X element used to tune the carrier concentration [95]. We note that most Chevrel phases experimentally studied in literature (i.e. $TiMo_6Se_8$) are not found in this screening because their computed energy above hull is higher than the considered threshold of 0.05 eV. We also note that most TE experimental work has focused on Chevrels with X as a transition metal. Our work suggests that reinvestigating Chevrel phases with alkali-earth and rare-earth elements might be of interest. For instance, $Ca(Mo_3S_4)_2$ emerges from our screening and could have its carrier concentration tuned by substituting Ca by La.

Although our screening likely discards potentially interesting phases, it also finds additional ones which were not reported in the literature as TE materials; therefore, these unreported phases may be candidates for further study. Among them our eyes fall on $PbMo_6S_8$, a known superconductor with a unique band structure containing a highly-pocketed valence band and the highest computed optimal PF among the Chevrels (see SI Fig. 23).

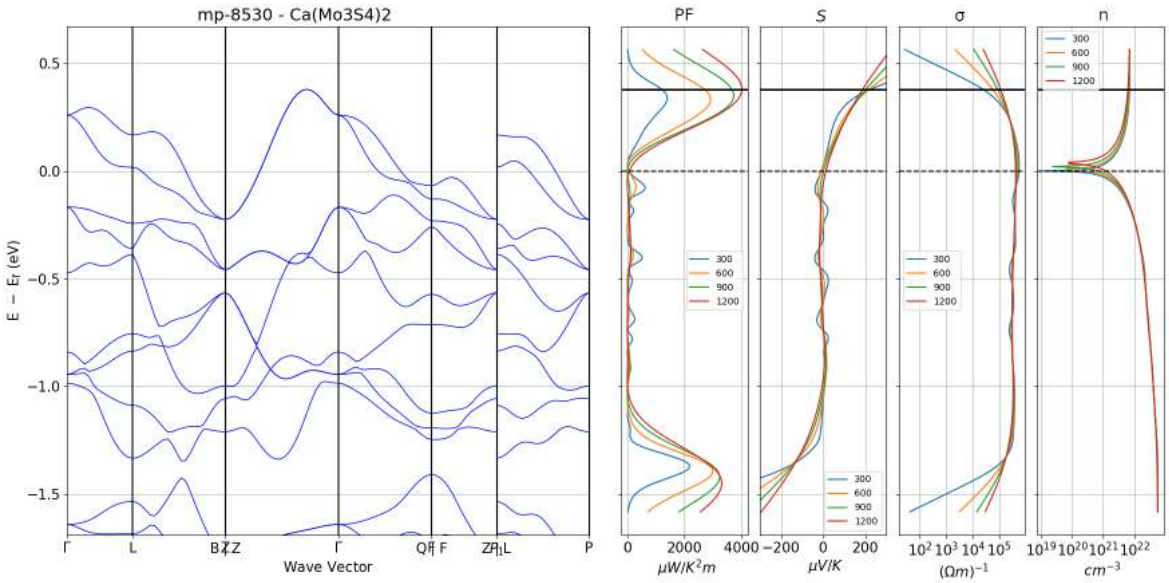

Figure 9: Band structure and calculated transport properties of $Ca(Mo_3S_4)_2$ (mp-8530).

Cu-containing

Cu_3SbS_3 (Fig. 10 and Fig. 12) is found to have a calculated optimal zT∼1.4 and to be slightly unstable (energy above Hull about 0.04 eV). As reported recently in Ref. [96], this compound was stabilized in the cubic structure by doping with Fe and tuning the hole carriers by Sb doping. The zT was measured to be 0.8 at 600 K. $Cu_{12}Sb_4S_{13}$ (SI Fig. 24) was reported in Ref. [97] to have a p-type metallic behavior and a zT∼0.4 at 600 K. The calculated optimal zT is ∼1, with a $\kappa_{\min}$ very close to the experimental lattice thermal conductivity at 600 K, predicted Seebeck slightly overestimated and σ and κ_{el} underestimated. Cu_3SbX_3 (X = S, Se) (SI Fig. 25) were found in the screening, but experimentally they are reported as semiconductors which must be doped to achieve reasonable p-type TE performance. Including spin-orbit coupling (SOC) [98] or using HSE [99] in the calculation opens a band gap in the band structure. Cu_2SnTe_3 (SI Fig. 26) has also been reported to be a standard semiconductor with a band gap opening at the Fermi level when HSE is used to calculate the band structure [100]. These two cases demonstrate one of the limits of our screening for the cases where the SOC and the exchange-correlation term dominates the characteristics of the bands.

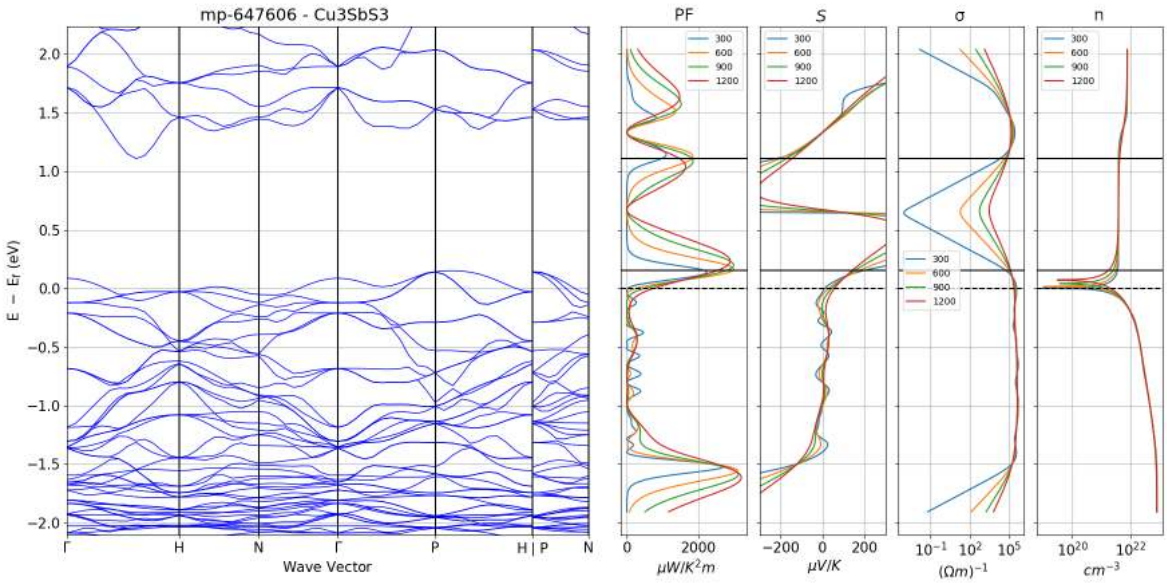

Figure 10: Band structure and calculated transport properties of Cu_3SbS_3 (mp-647606).

Others

Ta_3SiTe_6 (Fig. 11), a layered ternary telluride with a stacking (as shown in Fig. 12) similar to that of MoS_2, has been recently proposed as a topological semimetal. This material experimentally shows the typical metallic dependence of resistivity on temperature, and its Hall measurements show that hole carriers dominate the transport [101]. Another study focused on the band crossing at Fermi level provided evidence of its semimetallic nature combining ARPES measurements and ab-initio band structure calculations [102, 103]. Both studies do not mention the presence of the near band gap and its potential effect on the Seebeck coefficient. $Li_{12}Mg_3Si_4$ and Ca_3CrN_3 have been identified as potential electrides in Refs. [104] and [38], respectively. However, since these classes of materials are usually less stable at high temperatures, they might not be suitable for TE applications.

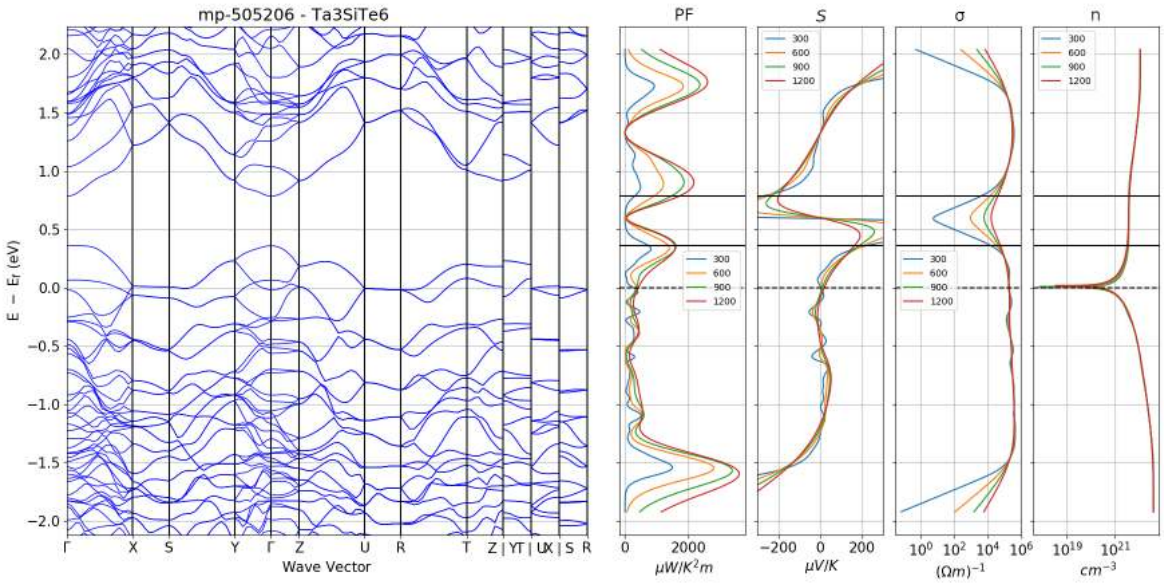

Figure 11: Band structure and calculated transport properties of Ta_3SiTe_6 (mp-505206).

High predicted zT oxides are also found in this screening: $Li_4(CuO_2)_3$ (SI Fig. 27) $La_3Ti_4O_{12}$ (SI Fig. 28), $Co(BiO_3)_2$ (SI Fig. 29), $Na_3(CuO_2)_2$ (SI Fig. 30), $LiNi_3O_4$ (SI Fig. 32). These oxides have theoretically predicted structures and no transport properties are reported in literature. Pr_2SbO_2 (SI Fig. 31) was synthesized in the orthorhombic phase, resulting in a semiconductor [105] whose TE properties were investigated experimentally in its family RE_2SbO_2 [106].

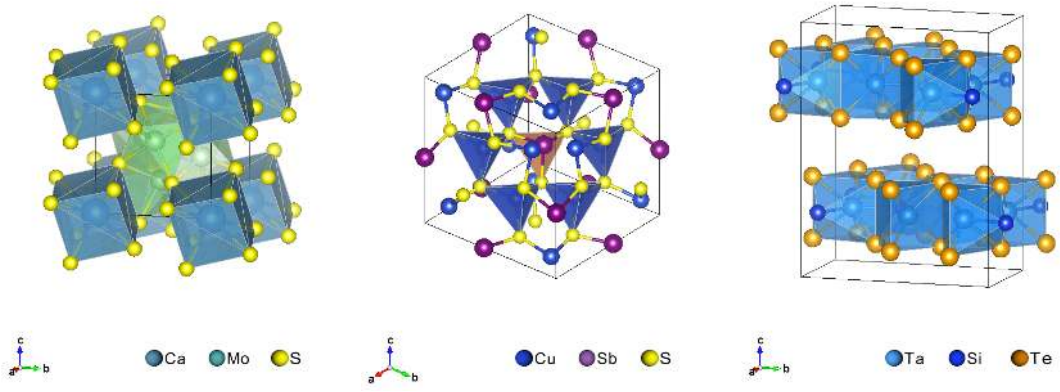

Figure 12: From left to right, the crystal structure of $Ca(Mo_3S_4)_2$, Cu_3SbS_3, and Ta_3SiTe_6.

A series of interesting gapped metals found in this screening but not reported in literature as TE materials are listed in the last two sections of Table 4. Their band structures and transport properties are reported from Fig. 33 of Sec. 7.2 of SI.

4 Conclusions

We have reported on a HT screening to search for gapped metals with attractive thermoelectric properties. By scanning the band structures and the transport properties in the MP database, it has been found that the key feature of these metals, i.e. a band gap near the Fermi level, is a quite common feature. The presence of this band gap has been discussed as crucial for enhancing the TE performance of these metals, making them comparable to semiconductors. Although, many of the gapped metals found here are already reported in the literature as TE materials, the present analysis represents the opportunity to review all these well-known compounds in the context of the gapped metals concept. Also, other interesting but less studied compounds emerged and are proposed for further investigations. Finally, given that the key feature of the band structure could be potentially exploited for other applications, the present report on gapped metals could also be of great value in other material science fields.

5 Acknowledgment

F.R. and G.-M.R. acknowledge support from the "Low Cost ThermoElectric Devices" (LOCOTED) project funded by the Région Wallonne (Programmes FEDER). G.H. and G.-M.R. are grateful to the F.R.S.-FNRS for financial support through the PDR Grants HTBaSE (T.1071.15). Computational resources were provided by the supercomputing facilities of the UCLouvain (CISM) and the Consortium des Equipements de Calcul Intensif en Fédération Wallonie-Bruxelles (CECI) funded by the Fonds de la Recherche Scientifique de Belgique (F.R.S.- FNRS) under convention No. 2.5020.11. A.D. and A.J. were supported by the U.S. Department of Energy, Office of Basic Energy Sciences, Early Career Research Program.

References

[1] T. M. Tritt and M. A. Subramanian, "Thermoelectric Materials, Phenomena, and Applications: A Bird's Eye View," *MRS Bulletin*, vol. 31, no. March, 2006.

[2] L. E. Bell, "Cooling, heating, generating power, and recovering waste heat with thermoelectric systems," *Science*, vol. 321, no. 5895, pp. 1457–1461, 2008.

[3] D. Champier, "Thermoelectric generators: A review of applications," *Energy Conversion and Management*, vol. 140, pp. 167–181, 2017.

[4] L. D. Zhao, S. H. Lo, Y. Zhang, H. Sun, G. Tan, C. Uher, C. Wolverton, V. P. Dravid, and M. G. Kanatzidis, "Ultralow thermal conductivity and high thermoelectric figure of merit in SnSe crystals," *Nature*, vol. 508, no. 7496, pp. 373–377, 2014.

[5] C. Gayner and K. K. Kar, "Recent advances in thermoelectric materials," *Progress in Materials Science*, vol. 83, pp. 330–382, 2016.

[6] G. Tan, L.-d. D. Zhao, and M. G. Kanatzidis, "Rationally Designing High-Performance Bulk Thermoelectric Materials," *Chemical Reviews*, vol. 116, no. 19, pp. 12123–12149, 2016.

[7] G. J. Snyder and E. S. Toberer, "Complex thermoelectric materials," *Materials for Sustainable Energy: A Collection of Peer-Reviewed Research and Review Articles from Nature Publishing Group*, vol. 7, no. February, pp. 101–110, 2010.

[8] Y. Pei, H. Wang, and G. J. Snyder, "Band engineering of thermoelectric materials," *Advanced Materials*, vol. 24, no. 46, pp. 6125–6135, 2012.

[9] X. Zhou, Y. Yan, X. Lu, H. Zhu, X. Han, G. Chen, and Z. Ren, "Routes for high-performance thermoelectric materials," *Materials Today*, vol. xxx, no. xx, pp. 1–15, 2018.

[10] J. Xin, Y. Tang, Y. Liu, X. Zhao, H. Pan, and T. Zhu, "Valleytronics in thermoelectric materials," *npj Quantum Materials*, vol. 3, no. 1, p. 9, 2018.

[11] K. B. Masood, P. Kumar, R. A. Singh, and J. Singh, "Odyssey of thermoelectric materials: foundation of the complex structure," *Journal of Physics Communications*, vol. 2, no. 6, p. 062001, 2018.

[12] S. Roychowdhury, M. Samanta, S. Perumal, and K. Biswas, "Germanium chalcogenide thermoelectrics: Electronic structure modulation and low lattice thermal conductivity," *Chemistry of Materials*, vol. 30, no. 17, pp. 5799–5813, 2018.

[13] A. Banik, S. Roychowdhury, and K. Biswas, "The journey of tin chalcogenides towards high-performance thermoelectrics and topological materials," *Chem. Commun.*, vol. 54, pp. 6573–6590, 2018.

[14] M. Samanta, T. Ghosh, S. Chandra, and K. Biswas, "Layered materials with 2d connectivity for thermoelectric energy conversion," *J. Mater. Chem. A*, vol. 8, pp. 12226–12261, 2020.

[15] A. F. May, D. J. Singh, and G. J. Snyder, "Influence of band structure on the large thermoelectric performance of lanthanum telluride," *Physical Review B - Condensed Matter and Materials Physics*, vol. 79, no. 15, pp. 1–4, 2009.

[16] F. Gascoin, J. Rasmussen, and G. J. Snyder, "High temperature thermoelectric properties of $Mo_3Sb_{7-x}Te_x$ for x = 1.6 and 1.5," *Journal of Alloys and Compounds*, vol. 427, no. 1-2, pp. 324–329, 2007.

[17] E. S. Toberer, S. R. Brown, T. Ikeda, S. M. Kauzlarich, and G. J. Snyder, "High thermoelectric efficiency in lanthanum doped $Yb_{14}MnSb_{11}$," *Applied Physics Letters*, vol. 93, no. 6, pp. 18–21, 2008.

[18] Y. Hu, J. Wang, A. Kawamura, K. Kovnir, and S. M. Kauzlarich, "$Yb_{14}MgSb_{11}$ and $Ca_{14}MgSb_{11}$ - New Mg-containing zintl compounds and their structures, bonding, and thermoelectric properties," *Chemistry of Materials*, vol. 27, no. 1, pp. 343–351, 2015.

[19] E. S. Toberer, C. A. Cox, S. R. Brown, T. Ikeda, A. F. May, S. M. Kauzlarich, and G. J. Snyder, "Traversing the Metal-Insulator Transition in a Zintl Phase: Rational Enhancement of Thermoelectric Efficiency in $Yb_{14}Mn_{1-x}Al_xSb_{11}$," *Advanced Functional Materials*, vol. 18, no. 18, pp. 2795–2800, 2008.

[20] S. R. Brown, S. M. Kauzlarich, F. Gascoin, and G. J. Snyder, "$Yb_{14}MnSb_{11}$: New High Efficiency Thermoelectric Material for Power Generation.," *ChemInform*, vol. 37, no. 25, pp. 1873–1877, 2006.

[21] C. A. Cox, E. S. Toberer, A. A. Levchenko, S. R. Brown, G. J. Snyder, A. Navrotsky, and S. M. Kauzlarich, "Structure, Heat Capacity, and High-Temperature Thermal Properties of $Yb_{14}Mn_{1-x}Al_xSb_{11}$," *Chemistry of Materials*, vol. 21, no. 7, pp. 1354–1360, 2009.

[22] L. Huang, R. He, S. Chen, H. Zhang, K. Dahal, H. Zhou, H. Wang, Q. Zhang, and Z. Ren, "A New n-type Half-Heusler Thermoelectric Material NbCoSb," *Materials Research Bulletin*, vol. 70, no. June, pp. 773–778, 2015.

[23] W. G. Zeier, S. Anand, L. Huang, R. He, H. Zhang, Z. Ren, C. Wolverton, and G. J. Snyder, "Using the 18-Electron Rule To Understand the Nominal 19-Electron Half-Heusler NbCoSb with Nb Vacancies," *Chemistry of Materials*, vol. 29, pp. 1210–1217, feb 2017.

[24] O. I. Malyi, M. T. Yeung, K. R. Poeppelmeier, C. Persson, and A. Zunger, "Spontaneous Non-stoichiometry and Ordering in Degenerate but Gapped Transparent Conductors," *Matter*, vol. 1, no. 1, pp. 280–294, 2019.

[25] M. Jonson and G. D. Mahan, "Mott's formula for the thermopower and the Wiedemann-Franz law," *Physical Review B*, vol. 21, no. 10, pp. 4223–4229, 1980.

[26] A. F. May, J.-P. P. Fleurial, and G. J. Snyder, "Thermoelectric performance of lanthanum telluride produced via mechanical alloying," *Physical Review B - Condensed Matter and Materials Physics*, vol. 78, no. 12, pp. 1–12, 2008.

[27] S. M. Kauzlarich, S. R. Brown, G. Jeffrey Snyder, R. Brown, and G. J. Snyder, "Zintl phases for thermoelectric devices," *Dalton Transactions*, no. 21, p. 2099, 2007.

[28] I. R. Fisher, S. L. Bud'ko, C. Song, P. C. Canfield, T. C. Ozawa, and S. M. Kauzlarich, "$Yb_{14}ZnSb_{11}$: charge balance in Zintl compounds as a route to intermediate Yb valence," *Physical Review Letters*, vol. 85, no. 5, pp. 1120–1123, 2000.

[29] S. Anand, K. Xia, V. I. Hegde, U. Aydemir, V. Kocevski, T. Zhu, C. Wolverton, and G. J. Snyder, "A valence balanced rule for discovery of 18-electron half-Heuslers with defects," *Energy and Environmental Science*, vol. 11, no. 6, pp. 1480–1488, 2018.

[30] H. Zhang, Y. Wang, L. Huang, S. Chen, H. Dahal, D. Wang, and Z. Ren, "Synthesis and thermoelectric properties of n-type half-Heusler compound VCoSb with valence electron count of 19," *Journal of Alloys and Compounds*, vol. 654, pp. 321–326, 2016.

[31] D. Parker, A. F. May, H. Wang, M. A. McGuire, B. C. Sales, and D. J. Singh, "Electronic and thermoelectric properties of CoSbS and FeSbS," *Physical Review B - Condensed Matter and Materials Physics*, vol. 87, no. 4, pp. 1–8, 2013.

[32] M. Miyata, T. Ozaki, S. Nishino, and M. Koyano, "Thermoelectric properties of high power factor sulfide NiSbS and Co substitution system $Ni_{1-x}Co_xSbS$," *Japanese Journal of Applied Physics*, vol. 56, p. 021801, feb 2017.

[33] A. Jain, S. P. Ong, G. Hautier, W. Chen, W. D. Richards, S. Dacek, S. Cholia, D. Gunter, D. Skinner, G. Ceder, and K. a. Persson, "The Materials Project: A materials genome approach to accelerating materials innovation," *APL Materials*, vol. 1, no. 1, p. 011002, 2013.

[34] J. E. Saal, S. Kirklin, M. Aykol, B. Meredig, and C. Wolverton, "Materials design and discovery with high-throughput density functional theory: The open quantum materials database (oqmd)," *JOM*, vol. 65, no. 11, pp. 1501–1509, 2013.

[35] W. Setyawan and S. Curtarolo, "High-throughput electronic band structure calculations: Challenges and tools," *Computational Materials Science*, vol. 49, no. 2, pp. 299 – 312, 2010.

[36] S. Curtarolo, G. L. Hart, M. B. Nardelli, N. Mingo, S. Sanvito, and O. Levy, "The high-throughput highway to computational materials design," *Nature Materials*, vol. 12, no. 3, pp. 191–201, 2013.

[37] A. Jain, Y. Shin, and K. A. Persson, "Computational predictions of energy materials using density functional theory," *Nature Reviews Materials*, vol. 1, p. 15004, Jan 2016. Review Article.

[38] L. A. Burton, F. Ricci, W. Chen, G. M. Rignanese, and G. Hautier, "High-Throughput Identification of Electrides from All Known Inorganic Materials," *Chemistry of Materials*, vol. 30, no. 21, pp. 7521–7526, 2018.

[39] G. K. H. Madsen, "Automated search for new thermoelectric materials: The case of LiZnSb," *Journal of the American Chemical Society*, vol. 128, no. 37, pp. 12140–12146, 2006.

[40] W. Chen, J.-H. Pöhls, G. Hautier, D. Broberg, S. Bajaj, U. Aydemir, Z. M. Gibbs, H. Zhu, M. Asta, G. J. Snyder, B. Meredig, M. A. White, K. Persson, and A. Jain, "Understanding thermoelectric properties from high-throughput calculations: trends, insights, and comparisons with experiment," *J. Mater. Chem. C*, vol. 4, pp. 4414–4426, 2016.

[41] D. Broberg, W. Chen, A. Jain, M. A. White, M. Asta, G. J. Snyder, and K. Persson, "$TmAgTe_2$ and XYZ_2 compounds , a new group of," *Journal of Materials Chemistry C*, 2015.

[42] P. Gorai, P. Parilla, E. S. Toberer, and V. Stevanović, "Computational Exploration of the Binary A1B1 Chemical Space for Thermoelectric Performance," *Chemistry of Materials*, vol. 27, no. 18, pp. 6213–6221, 2015.

[43] Carrete Jesús, W. Li, N. Mingo, S. Wang, and S. Curtarolo, "Finding unprecedentedly low-thermal-conductivity half-heusler semiconductors via high-throughput materials modeling," *Physical Review X*, vol. 4, pp. 1–9, feb 2014.

[44] J. M. Rondinelli and S. J. May, "Deliberate Deficiencies: Expanding Electronic Function through Non-stoichiometry," *Matter*, vol. 1, no. 1, pp. 33–35, 2019.

[45] K. R. Poeppelmeier and J. M. Rondinelli, "Correlated oxides: Metals amassing transparency," *Nature Materials*, vol. 15, no. 2, pp. 132–134, 2016.

[46] D. Zhang, J. Yang, Q. Jiang, L. Fu, Y. Xiao, Y. Luo, and Z. Zhou, "Improvement of thermoelectric properties of Cu_3SbSe_4 compound by In doping," *Materials and Design*, vol. 98, pp. 150–154, 2016.

[47] X. Zhang, L. Zhang, J. D. Perkins, and A. Zunger, "Intrinsic Transparent Conductors without Doping," *Physical Review Letters*, vol. 115, no. 17, 2015.

[48] M. N. Gjerding, M. Pandey, and K. S. Thygesen, "Band structure engineered layered metals for low-loss plasmonics," *Nature Communications*, vol. 8, pp. 1–8, 2017.

[49] F. Ricci, W. Chen, U. Aydemir, G. J. Snyder, G.-M. Rignanese, A. Jain, and G. Hautier, "An ab initio electronic transport database for inorganic materials," *Scientific Data*, vol. 4, p. 170085, 2017.

[50] K. Mathew, J. H. Montoya, A. Faghaninia, S. Dwarakanath, M. Aykol, H. Tang, I. heng Chu, T. Smidt, B. Bocklund, M. Horton, J. Dagdelen, B. Wood, Z.-K. Liu, J. Neaton, S. P. Ong, K. Persson, and A. Jain, "Atomate: A high-level interface to generate, execute, and analyze computational materials science workflows," *Computational Materials Science*, vol. 139, pp. 140 – 152, 2017.

[51] G. Hautier, S. P. Ong, A. Jain, C. J. Moore, and G. Ceder, "Accuracy of density functional theory in predicting formation energies of ternary oxides from binary oxides and its implication on phase stability," *Phys. Rev. B*, vol. 85, p. 155208, Apr 2012.

[52] G. K. Madsen and D. J. Singh, "BoltzTraP. A code for calculating band-structure dependent quantities," *Computer Physics Communications*, vol. 175, no. 1, pp. 67–71, 2006.

[53] M. de Jong, W. Chen, T. Angsten, A. Jain, R. Notestine, A. Gamst, M. Sluiter, C. Krishna Ande, S. van der Zwaag, J. J. Plata, C. Toher, S. Curtarolo, G. Ceder, K. A. Persson, and M. Asta, "Charting the complete elastic properties of inorganic crystalline compounds," *Scientific Data*, vol. 2, p. 150009, 2015.

[54] L. Ward, A. Dunn, A. Faghaninia, N. E. Zimmermann, S. Bajaj, Q. Wang, J. Montoya, J. Chen, K. Bystrom, M. Dylla, K. Chard, M. Asta, K. A. Persson, G. J. Snyder, I. Foster, and A. Jain, "Matminer: An open source toolkit for materials data mining," *Computational Materials Science*, vol. 152, pp. 60 – 69, 2018.

[55] https://github.com/hackingmaterials/automatminer.

[56] A. Dunn, Q. Wang, A. Ganose, D. Dopp, and A. Jain, "Benchmarking materials property prediction methods: The matbench test set and automatminer reference algorithm," 2020.

[57] L. Ward, A. Agrawal, A. Choudhary, and C. Wolverton, "A general-purpose machine learning framework for predicting properties of inorganic materials," *npj Computational Materials*, vol. 2, p. 16028, 2016.

[58] A. M. Deml, R. O'Hayre, C. Wolverton, and V. Stevanovic, "Cheminform abstract: Predicting density functional theory total energies and enthalpies of formation of metal-nonmetal compounds by linear regression," *ChemInform*, vol. 47, no. 44, 2016.

[59] F. Faber, A. Lindmaa, O. A. Von Lilienfeld, and R. Armiento, "Crystal structure representations for machine learning models of formation energies," *International Journal of Quantum Chemistry*, vol. 115, no. 16, pp. 1094–1101, 2015.

[60] D. G. Cahill and R. O. Pohl, "Lattice vibrations and heat transport in crystals and glasses," *Annual Review of Physical Chemistry*, vol. 39, no. 1, pp. 93–121, 1988.

[61] D. G. Cahill, S. K. Watson, and R. O. Pohl, "Lower limit to the thermal conductivity of disordered crystals," *Phys. Rev. B*, vol. 46, pp. 6131–6140, Sep 1992.

[62] W. Setyawan, R. M. Gaume, S. Lam, R. S. Feigelson, and S. Curtarolo, "High-throughput combinatorial database of electronic band structures for inorganic scintillator materials," *ACS Combinatorial Science*, vol. 13, no. 4, pp. 382–390, 2011.

[63] D. Cheikh, B. E. Hogan, T. Vo, P. Von Allmen, K. Lee, D. M. Smiadak, A. Zevalkink, B. S. Dunn, J.-p. Fleurial, and S. K. Bux, "Praseodymium Telluride: A High-Temperature, High-ZT Thermoelectric Material," *Joule*, vol. 2, pp. 698–709, apr 2018.

[64] A. P. Holm, T. C. Ozawa, S. M. Kauzlarich, S. A. Morton, G. D. Waddill], and J. G. Tobin, "X-ray photoelectron spectroscopy studies of yb14mnsb11 and yb14znsb11," *Journal of Solid State Chemistry*, vol. 178, no. 1, pp. 262 – 269, 2005.

[65] S. M. Kauzlarich and F. Sui, *Light Element Group 13-14 Clathrate Phases*, pp. 227–248. Dordrecht: Springer Netherlands, 2014.

[66] M. Christensen, S. Johnsen, and B. B. Iversen, "Thermoelectric clathrates of type I," *Dalton Transactions*, vol. 39, no. 4, pp. 978–992, 2010.

[67] H. Kleinke, "New bulk materials for thermoelectric power generation: Clathrates and complex antimonides," *Chemistry of Materials*, vol. 22, no. 3, pp. 604–611, 2010.

[68] G. A. Slack, "Design concepts for improved thermoelectric materials," *MRS Proceedings*, vol. 478, p. 47, 1997.

[69] A. Saramat, G. Svensson, A. E. Palmqvist, C. Stiewe, E. Mueller, D. Platzek, S. G. Williams, D. M. Rowe, J. D. Bryan, and G. D. Stucky, "Large thermoelectric figure of merit at high temperature in Czochralski-grown clathrate $Ba_8Ga_{16}Ge_{30}$," *Journal of Applied Physics*, vol. 99, no. 2, 2006.

[70] C. W. Myles, J. Dong, and O. F. Sankey, "Structural and electronic properties of tin clathrate materials," *Physical Review B - Condensed Matter and Materials Physics*, vol. 64, no. 16, pp. 1–11, 2001.

[71] M. Iioka, H. Udono, M. Imai, and M. Aoki, " Band structure characterization of $K_8Ga_8Si_{38}$ clathrates by optical measurement ," *JJAP Conf. Proc.*, vol. 3, p. 011201, 2016.

[72] M. Falmbigl, M. X. Chen, A. Grytsiv, P. Rogl, E. Royanian, H. Michor, E. Bauer, R. Podloucky, and G. Giester, "Type-I clathrate $Ba_8Ni_xSi_{46-x}$: Phase relations, crystal chemistry and thermoelectric properties," *Dalton Transactions*, vol. 41, no. 29, pp. 8839–8849, 2012.

[73] X. Shi, J. Yang, S. Bai, J. Yang, H. Wang, M. Chi, J. R. Salvador, W. Zhang, L. Chen, and W. Wong-Ng, "On the design of high-efficiency thermoelectric clathrates through a systematic cross-substitution of framework elements," *Advanced Functional Materials*, vol. 20, no. 5, pp. 755–763, 2010.

[74] B. Owens-Baird, J. Wang, S. G. Wang, Y.-S. Chen, S. Lee, D. Donadio, and K. Kovnir, "Iii-v clathrate semiconductors with outstanding hole mobility: $Cs_8In_{27}Sb_{19}$ and $A_8Ga_{27}Sb_{19}$ (a = cs, rb)," *Journal of the American Chemical Society*, vol. 142, no. 4, pp. 2031–2041, 2020.

[75] M. Naito and S. Tanaka, "Electrical Transport Properties in 2H-NbS_2, -$NbSe_2$, -TaS_2, and -$TaSe_2$," *Journal of the Physical Society of Japan*, vol. 51, pp. 219–227, jan 1982.

[76] N. F. Hinsche and K. S. Thygesen, "Electron-phonon interaction and transport properties of metallic bulk and monolayer transition metal dichalcogenide TaS_2," *2D Materials*, vol. 5, no. 1, 2018.

[77] J. Molenda, T. Bak, and J. Marzec, "Electrical and electrochemical properties of niobium disulphide," *Physica Status Solidi (a)*, vol. 156, no. 1, pp. 159–168, 1996.

[78] M. Beaumale, T. Barbier, Y. Bréard, S. Hébert, Y. Kinemuchi, and E. Guilmeau, "Thermoelectric properties in the series $Ti_{1-x}Ta_xS_2$," *Journal of Applied Physics*, vol. 115, no. 4, 2014.

[79] B. Li, A. V. Mudring, and J. D. Corbett, "Valence Compounds versus Metals. Synthesis, Characterization, and Electronic Structures of Cubic Ae_4Pn_3 Phases in the Systems Ae = Ca, Sr, Ba, Eu; Pn = As, Sb, Bi," *Inorganic Chemistry*, vol. 42, no. 21, pp. 6940–6945, 2003.

[80] O. I. Malyi, G. M. Dalpian, X.-G. Zhao, Z. Wang, and A. Zunger, "Realization of predicted exotic materials: The burden of proof," *Materials Today*, 2019.

[81] B. Bradlyn, J. Cano, Z. Wang, M. G. Vergniory, C. Felser, R. J. Cava, and B. A. Bernevig, "Beyond dirac and weyl fermions: Unconventional quasiparticles in conventional crystals," *Science*, vol. 353, no. 6299, 2016.

[82] N. Haldolaarachchige, W. A. Phelan, Y. M. Xiong, R. Jin, J. Y. Chan, S. Stadler, and D. P. Young, "Thermoelectric properties of intermetallic semiconducting $RuIn_3$ and metallic $IrIn_3$," *Journal of Applied Physics*, vol. 113, no. 8, pp. 1–6, 2013.

[83] T. Y. Ou-Yang, G. J. Shu, and H. R. Fuh, "Thermoelectric performance and electronic properties of transition metal monosilicides," *EPL (Europhysics Letters)*, vol. 120, p. 17002, oct 2017.

[84] M. Kosaka, S. Ottomo, A. Machida, T. Kirigane, R. Numakura, S. Katano, and S. Michimura, "Magnetic and transport properties of the narrow-gap semiconductor Yb_5Si_4," *Journal of Physics: Conference Series*, vol. 592, no. 1, 2014.

[85] M. Gu, Z. Wang, J. G. Connell, D. E. Perea, L. J. Lauhon, F. Gao, and C. Wang, "Electronic origin for the phase transition from amorphous Li_xSi to crystalline $Li_{15}Si_4$," *ACS Nano*, vol. 7, no. 7, pp. 6303–6309, 2013.

[86] R. Chevrel, M. Sergent, and J. Prigent, "Sur de nouvelles phases sulfurées ternaires du molybdène," *Journal of Solid State Chemistry*, vol. 3, no. 4, pp. 515 – 519, 1971.

[87] O. Peña, "Chevrel phases: Past, present and future," *Physica C: Superconductivity and its Applications*, vol. 514, pp. 95–112, 2015.

[88] T. Caillat, J. P. Fleurial, and G. J. Snyder, "Potential of Chevrel phases for thermoelectric applications," *Solid State Sciences*, vol. 1, no. 7-8, pp. 535–544, 1999.

[89] Y. Ohta, J. Rousseau, J. Tobola, P. Pecheur, H. Scherrer, I. Iwanaga, A. Kasama, and Y. Matsumura, "Thermoelectric properties of Mo_6Se_8-based chevrel phase with semiconducting properties," in *Proceedings ICT'03. 22nd International Conference on Thermoelectrics (IEEE Cat. No.03TH8726)*, pp. 255–258, 2003.

[90] J. Tobola, P. Pecheur, H. Scherrer, S. Kaprzyk, Y. Ohta, and Y. Matsumura, "The electronic structure of MxMo6se8 chevrel phases with defects," *Journal of Physics: Condensed Matter*, vol. 15, pp. L655–L659, oct 2003.

[91] M. Ohta, H. Obara, and A. Yamamoto, "Preparation and thermoelectric properties of chevrel-phase $Cu_xMo_6S_8$ $(2.0 \leq x \leq 4.0)$," *Materials Transactions*, vol. 50, no. 9, pp. 2129–2133, 2009. cited By 26.

[92] M. Ohta, A. Yamamoto, and H. Obara, "Thermoelectric properties of chevrel-phase sulfides $M_xMo_6S_8$ (m: Cr, mn, fe, ni)," *Journal of Electronic Materials*, vol. 39, no. 9, pp. 2117–2121, 2010. cited By 11.

[93] M. McGuire, A. Schmidt, F. Gascoin, G. Jeffrey Snyder, and F. DiSalvo, "Thermoelectric and structural properties of a new chevrel phase: $Ti_0 \cdot 3\,Mo_5RuSe_8$," *Journal of Solid State Chemistry*, vol. 179, no. 7, pp. 2158–2163, 2006. cited By 13.

[94] P. Afanasiev and I. Bezverkhyy, "Ternary transition metals sulfides in hydrotreating catalysis," *Applied Catalysis A: General*, vol. 322, pp. 129 – 141, 2007. Active Phases for Hydrotreating Catalysis.

[95] R. W. Nunes, I. I. Mazin, and D. J. Singh, "Theoretical search for chevrel-phase-based thermoelectric materials," *Phys. Rev. B*, vol. 59, pp. 7969–7972, Mar 1999.

[96] B. Du, R. Zhang, M. Liu, K. Chen, H. Zhang, and M. J. Reece, "Crystal structure and improved thermoelectric performance of iron stabilized cubic Cu_3SbS_3 compound," *Journal of Materials Chemistry C*, vol. 7, no. 2, pp. 394–404, 2019.

[97] P. Levinsky, C. Candolfi, A. Dauscher, J. Tobola, J. Hejtmánek, and B. Lenoir, "Thermoelectric properties of the tetrahedrite-tennantite solid solutions $Cu_{12}Sb_{4-x}As_xS_{13}$ and $Cu_{10}Co_2Sb_{4-y}As_yS_{13}$ ($0 \leq$ x, y ≤ 4)," *Physical Chemistry Chemical Physics*, vol. 21, no. 8, pp. 4547–4555, 2019.

[98] B. Xu, X. Zhang, Y. Sun, J. Zhang, Y. Wang, and L. Yi, "Elastic anisotropy and anisotropic transport properties of Cu_3SbSe_4 and Cu_3SbS_4," *Journal of the Physical Society of Japan*, vol. 83, no. 9, pp. 1–8, 2014.

[99] G. García, P. Palacios, A. Cabot, and P. Wahnón, "Thermoelectric Properties of Doped-Cu_3SbSe_4 Compounds: A First-Principles Insight," *Inorganic Chemistry*, vol. 57, no. 12, pp. 7321–7333, 2018.

[100] A. Shigemi, T. Maeda, and T. Wada, "First-principles calculation of Cu_2SnS_3 and related compounds," *Physica Status Solidi (B) Basic Research*, vol. 252, pp. 1230–1234, jun 2015.

[101] M. Naveed, F. Fei, H. Bu, X. Bo, S. A. Shah, B. Chen, Y. Zhang, Q. Liu, B. Wei, S. Zhang, C. Xi, X. Wan, and F. Song, "Magneto-transport and Shubnikov-de Haas oscillations in the layered ternary telluride Ta_3SiTe_6 topological semimetal," *arXiv*, 2019.

[102] T. Sato, Z. Wang, K. Nakayama, S. Souma, D. Takane, Y. Nakata, H. Iwasawa, C. Cacho, T. Kim, T. Takahashi, and Y. Ando, "Observation of band crossings protected by nonsymmorphic symmetry in the layered ternary telluride Ta_3SiTe_6," *Physical Review B*, vol. 98, no. 12, pp. 1–6, 2018.

[103] S. Li, Y. Liu, S. S. Wang, Z. M. Yu, S. Guan, X. L. Sheng, Y. Yao, and S. A. Yang, "Nonsymmorphic-symmetry-protected hourglass Dirac loop, nodal line, and Dirac point in bulk and monolayer X_3SiTe_6 (X = Ta, Nb)," *Physical Review B*, vol. 97, no. 4, pp. 1–11, 2018.

[104] J. Wang, Q. Zhu, Z. Wang, and H. Hosono, "Ternary inorganic electrides with mixed bonding," *Phys. Rev. B*, vol. 99, p. 064104, Feb 2019.

[105] O. V. Magdysyuk, J. Nuss, and M. Jansen, "Modulated crystal structure of Pr_2SbO_2," *Acta Crystallographica Section B*, vol. 69, pp. 547–555, Dec 2013.

[106] P. L. Wang, T. Kolodiazhnyi, J. Yao, and Y. Mozharivskyj, "Decoupling the electrical conductivity and seebeck coefficient in the Ṛ compounds through local structural perturbations," *Journal of the American Chemical Society*, vol. 134, no. 3, pp. 1426–1429, 2012.

MP_{id}	Formula	Spacegroup	type	zT	PF	κ_{el}	n	κ_{min}
Clathrates								
mp-27800	K_4Ge_{23}	$Pm\bar{3}n$	n	1.45	37.72	0.93	5.63	0.63
mp-186	Na_4Si_{23}	$Pm\bar{3}n$	n	0.95	30.98	0.76	7.09	1.19
mp-531	K_4Si_{23}	$Pm\bar{3}n$	n	0.83	28.04	0.81	6.7	1.22
mp-13909	K_4Sn_{23}	$Pm\bar{3}n$	n	1.37	26.17	0.81	3.79	0.34
mp-2496	Cs_4Sn_{23}	$Pm\bar{3}n$	n	1.61	25.89	0.65	3.74	0.31
TMDs								
mp-10033	NbS_2	$P6_3/mmc$	n	0.67	75.3	6.19	10.11	0.51
mp-1984	TaS_2	$P6_3/mmc$	n	0.28	42.62	8.77	10.09	0.44
mp-2207	$NbSe_2$	$P6_3/mmc$	p	0.09	15.43	10.26	10.01	0.39
mp-2156	TiS_2	$P\bar{3}m1$	p	0.44	57.16	7.24	1.71	0.57
La_3Te_4 family								
mp-23310	Yb_4Bi_3	$I\bar{4}3d$	p	0.71	13.59	0.82	4.35	0.32
mp-1295	Yb_4Sb_3	$I\bar{4}3d$	p	0.71	14.99	0.89	4.63	0.37
mp-30892	Ba_4Bi_3	$I\bar{4}3d$	p	0.89	14.57	0.75	3.12	0.23
mp-30893	Sr_4Bi_3	$I\bar{4}3d$	p	0.74	14.81	0.79	3.62	0.41
mp-1098	Yb_4As_3	$I\bar{4}3d$	p	0.7	16.85	1.0	5.56	0.45
Others								
mp-630976	In_3Ir	$P4_2/mnm$	n	1.16	33.57	1.24	9.48	0.49
mp-22236	In_3Co	$P4_2/mnm$	n	1.03	44.09	1.95	9.16	0.61
mp-20559	Ga_3Co	$P4_2/mnm$	n	0.51	41.57	3.94	10.15	0.91
mp-20101	Yb_5Si_4	Pnma	p	0.76	12.23	0.41	8.6	0.55
mp-21300	Yb_5Ge_4	Pnma	p	0.84	11.96	0.4	8.53	0.46
mp-569849	$Li_{15}Si_4$	$I\bar{4}3d$	p	0.41	28.39	2.83	2.42	1.36
mp-24202	Th_4H_{15}	$I\bar{4}3d$	n	1.08	37.85	1.05	4.77	1.04
mp-1777	$Li_{15}Ge_4$	$I\bar{4}3d$	p	0.44	27.96	2.84	2.34	0.95
mp-676024	$Li_{27}Sb_{10}$	C2/m	p	1.2	54.32	2.03	3.97	0.7
mp-9546	Yb_2C_3	$I\bar{4}3d$	n	0.63	34.07	2.29	10.11	0.96
mp-29973	SrN	C2/m	n	0.43	20.76	2.21	10.06	0.68
mp-32727	Y_3Se_4	C2/m	n	0.5	24.73	2.45	4.95	0.52
mp-28424	K_4P_3	Cmcm	p	0.41	14.44	1.63	3.76	0.48
mp-624299	Cu_7S_4	Pnma	p	0.91	28.95	1.08	5.4	0.83

Table 3: Binary gapped metals with high computed optimal zT at 600 K. For each material, the optimal power factor (PF) in $\mu W/(K^2\ cm)$, the optimal carrier concentration (n) in 10^{21} cm^{-3}, and the thermal conductivity κ in W/(K m) are also reported. For the latter, κ_{el} is the calculated optimal electrical contribution and κ_{min} provides the minimum limit for the lattice contribution as obtained in the Cahill model. The figure of the crystal structure, the band structure, and the related calculated transport properties of all these compounds are provided in the SI.

MP_{id}	Formula	Spacegroup	type	zT	PF	κ_{el}	n	κ_{min}
Chevrels								
mp-8530	$Ca(Mo_3S_4)_2$	$R\bar{3}$	p	0.94	29.13	0.96	6.58	0.89
mp-3043	$Sr(Mo_3S_4)_2$	$R\bar{3}$	p	0.96	27.65	0.89	6.35	0.85
mp-555066	Mo_6PbS_8	$R\bar{3}$	p	1.0	32.25	1.14	6.2	0.79
mp-2945	$Yb(Mo_3S_4)_2$	$R\bar{3}$	p	0.96	29.33	1.02	6.63	0.82
Cu-containing								
mp-647606	Cu_3SbS_3	$I\bar{4}3m$	p	1.38	29.61	0.59	3.15	0.7
mp-647164	$Cu_{12}Sb_4S_{13}$	$I\bar{4}3m$	p	1.09	16.18	0.33	2.56	0.56
mp-5702	Cu_3SbS_4	$I\bar{4}2m$	p	0.58	38.13	3.21	10.07	0.72
mp-9814	Cu_3SbSe_4	$I\bar{4}2m$	p	1.24	43.37	1.57	10.0	0.53
mp-13089	Cu_2SnTe_3	Imm2	p	1.17	74.36	3.38	10.06	0.42
Others								
mp-505206	Ta_3SiTe_6	Pnma	p	1.29	13.87	0.34	3.32	0.3
mp-28754	Nb_3GeTe_6	Pnma	p	0.76	11.03	0.43	3.28	0.44
mp-505137	Nb_3SiTe_6	Pnma	p	0.95	12.45	0.33	3.33	0.46
mp-25248	$Li_4(CuO_2)_3$	C2/m	n	0.65	30.86	1.48	6.16	1.38
mp-754804	$La_3Ti_4O_{12}$	Amm2	n	0.65	53.02	3.48	2.53	1.45
mp-765403	$Co(BiO_3)_2$	P321	p	0.62	25.64	1.58	7.83	0.92
mp-559817	$Na_3(CuO_2)_2$	$P2_1/c$	n	0.61	34.77	2.41	7.01	1.01
mp-676273	Pr_2SbO_2	$P\bar{1}$	p	0.44	74.64	9.47	7.87	0.65
mp-755956	$LiNi_3O_4$	Cmmm	p	0.42	54.11	5.96	10.09	1.8
mp-11176	$Ca_3(SiIr)_4$	$I\bar{4}3m$	p	0.37	27.17	3.59	9.26	0.79
mp-22418	$Sr_3(SnIr)_4$	$I\bar{4}3m$	p	0.56	35.27	3.31	6.89	0.5
mp-27835	K_2OsBr_6	$Fm\bar{3}m$	p	2.46	46.33	0.93	5.7	0.2
mp-639910	$Y(Sn_3Ru_2)_2$	$I\bar{4}2m$	p	1.02	33.17	1.23	3.21	0.72
mp-36966	$NaSm_2Se_3$	C2/c	n	0.84	29.14	1.6	6.22	0.49
mp-37312	$Na(La_2Se_3)_4$	$I\bar{4}2d$	n	0.81	10.11	0.31	1.55	0.44
mp-753216	$LiAg_2F_4$	Cmce	p	0.81	49.82	2.98	8.38	0.71
mp-675367	Nb_3IrS_8	P1	n	0.73	46.27	3.06	6.33	0.72
mp-569313	$Mg_3Si_8Ir_3$	$F\bar{4}3m$	p	0.73	36.35	1.86	3.99	1.14
mp-8331	$Li_{12}Mg_3Si_4$	$I\bar{4}3d$	n	0.72	39.64	1.85	6.02	1.46
mp-4139	Nb_4GaS_8	$F\bar{4}3m$	n	0.6	19.4	1.14	3.41	0.8
mp-12906	Sr_3CrN_3	$P6_3/m$	n	0.68	13.68	0.45	6.49	0.76
mp-675056	$Na_3(TiS_2)_{10}$	Cm	n	0.45	26.16	2.66	3.89	0.81
mp-8670	Ca_3CrN_3	Cmcm	n	0.45	13.35	0.44	8.58	1.32

Table 4: Ternary gapped metals with high computed optimal zT at 600 K. For each material, the optimal power factor (PF) in $\mu W/(K^2\ cm)$, the optimal carrier concentration (n) in 10^{21} cm^{-3}, and the thermal conductivity κ in W/(K m) are also reported. For the latter, κ_{el} is the calculated optimal electrical contribution and κ_{min} provides the minimum limit for the lattice contribution as obtained in the Cahill model. The figure of the crystal structure, the band structure, and the related calculated transport properties for each compounds are provided in the SI.